Observation of surface enhanced IR absorption coefficient in alkanethiol based self-assembled monolayers on GaAs(001)

Gregory M. Marshall,[1,2] Farid Bensebaa,[2] and Jan J. Dubowski[1,a)]

[1]*Department of Electrical and Computer Engineering, Université de Sherbrooke, Sherbrooke, Québec J1K 2R1, Canada*
[2]*Institute for Chemical Process and Environmental Technology, National Research Council of Canada, Ottawa, Ontario K1A 0R6, Canada*

Alkanethiol self-assembled monolayers (SAMs) of various methylene group chain lengths $[HS-(CH_2)_n-CH_3]$ ($n=9,11,13,15,17$) were fabricated on the GaAs(001) surface followed by characterization using Fourier transform infrared spectroscopy. Modal analysis of the CH_2 stretching mode region ($2800-3000$ cm^{-1}) showed that linear scaling of the n-dependent factors accurately reproduced the spectral data, supporting a chain-length consistent physical model upon which a measurement of the absorption coefficient was based. Evaluated from the linearity of the absorbance data, a peak coefficient of 3.5×10^4 cm^{-1} was obtained and a domain for ordered self-assembly was assigned for values $n > 9$. Compared with measurements of the absorption coefficient made in the liquid phase, the SAM phase coefficient was determined to be about six times greater. This enhancement effect is discussed in terms of contributions relating to the locally ordered environment and is largely attributed to the chemical properties of the interface. We believe this to be the first demonstration of IR spectral enhancement of a molecular species chemisorbed on the semiconductor surface. © *2009 American Institute of Physics*. [DOI: 10.1063/1.3122052]

I. INTRODUCTION

The development of surface-molecule interface technology often depends on the effective control and characterization of self-assembly processes at interfaces where nanoscale effects may be exploited. Long-chain alkanethiol self-assembled monolayers (SAMs) on GaAs(001) have been studied in this context by a number of authors, both from the perspective of fundamental material science[1–10] and as a potential route to applications including surface passivation,[11] metal-molecule-semiconductor junctions,[12,13] the assembly of DNA hybridization probes,[14] and the immobilization of functional proteins such as avidin.[15] In these studies, Fourier transform infrared (FTIR) spectroscopy is frequently employed to investigate important SAM structural parameters such as molecular orientation[16] and the fraction of conformational defects.[17,18]

In an effort to further explore the nature of this material system, particularly with a view to developing benchmarks against which more complex functional interfaces may be compared, this paper investigates the absorption coefficient characteristics of alkanethiol SAMs prepared on the GaAs(001) surface. The absorption coefficient, typically derived from bulk phase Beer–Lambert measurements, may be used to determine other parameters of interest. For example, it may be cast in terms of the molar absorption ε (M^{-1} cm^{-1}) yielding the molar surface density ρ (mol cm^{-2}).[19,20] The complex optical dispersion properties of the SAM can also be approximated from bulk state absorption measurements using the Kramers–Kronig transformation,[20,21] and have been used to develop calculated SAM vibrational spectra.[18,21,22] The accuracy of such formulations depends on a correspondence from the bulk to the SAM phase that may not always be direct.[18,23] Consequently, we are motivated toward making a surface measurement of the absorption coefficient directly from the SAM phase.

Our analysis concerns the IR absorption characteristics of the CH_2 stretching mode region ($2800-3000$ cm^{-1}) for various chain-length n-alkanethiol $[HS-(CH_2)_n-CH_3]$ SAMs on semi-insulating (SI) GaAs(001). From transmission measurements, the absorption coefficient of the SAM phase is derived from the absorption amplitude linearized as a function of molecular chain length. Corresponding Beer–Lambert measurements made in the molecular liquid phase are then used for means of comparison. Note that SI-GaAs is well suited for transmission IR measurements of the SAM phase; because of their high extinction, doped GaAs or Si and Au substrates can only support grazing-angle reflection IR measurements, making absorption length evaluation more difficult. In this context, our results have relevance in the generalized domain of alkyl-SAMs prepared on a variety of substrates. The analysis continues with a discussion of the structural factors that contribute to the observed differences between liquid and SAM phase absorption coefficients. In addition, the absorption enhancement from possible surface and intermolecular effects is considered.

II. EXPERIMENTAL DETAILS

SI-GaAs(001) wafers were cleaned using 5 min sonication in each of Opticlear™, acetone, and isopropanol (IPA). Alkanethiol solutions in degassed ethanol were prepared at 2–3 mM concentration from each of the following: octade-

---

a)Electronic mail: jan.j.dubowski@usherbrooke.ca. Tel.: (819) 821-8000. FAX: (819) 821-7937.

canethiol (n17), hexadecanethiol (n15), tetradecanethiol (n13), dodecanethiol (n11), and decanethiol (n9), where the decade prefix refers to $n+1$ carbon atoms per molecule, accounting for the terminal CH_3 group. In addition, 50–100 mM of 28% NH_4OH/H_2O was added to each solution, according to sample preparation procedures described by McGuiness et al.[7] The GaAs wafers were then wet etched in 28% NH_4OH/H_2O for 2 min in order to remove surface oxides[7,24,25] followed by direct rinsing in degassed ethanol and subsequent immersion in the prepared solutions for 20 h. Following SAM-GaAs incubation, the samples were rinsed in IPA and dried in a nitrogen stream.[26]

Liquid phase samples of n9, n11, and n13 were prepared by wetting the neat liquid between two thin (150 μm) coverglass slides.[27] The thickness of the resulting liquid sandwich layer was measured (± 1 μm) by through-focus 200× optical microscopy (Leica DM-RXE), making use of small area voids around the layer, such that the interior surface features of the respective coverglass slides were resolved. The corresponding z-position readings were recorded from a digital translation stage and subtracted. Sample preparation ensured that a suitable void-free area was available for FTIR measurements.

Mid-IR spectra were recorded in transmission using a Bruker Optics Hyperion 2000 FTIR-microscope coupled to a Bruker Optics Tensor 27 spectrometer. The probing spot size was approximately 2 mm in diameter, the spectral resolution was set at 4 cm^{-1}, and continuous nitrogen purging of the sample glovebox was used. Spectra were recorded for freshly prepared samples, baselined through an etched GaAs reference wafer (incubated in ethanol as the control) such that the resulting difference spectrum revealed features specific to the SAM only. At least 3 min scanning time was required to achieve a good signal-to-noise ratio.

III. SPECTRUM MODAL ANALYSIS

Differential FTIR spectra for n17, n15, n13, n11, and n9 SAMs are provided in Fig. 1. Linear baseline subtraction and vertical spectrum shifts have been applied. Identifying characteristics are the CH_2 stretching mode peaks, located in the following ranges: (a) $2917-2921$ cm^{-1} (asymmetric mode) and (b) $2850-2851$ cm^{-1} (symmetric mode). Also visible is the CH_3 stretching mode at (c) associated with the terminal methyl group near 2959 cm^{-1}. In general terms, peak frequencies are expected to shift to higher energy values corresponding to the fraction of gauche defects where smaller chain lengths are used.[9,17,18] Note that an asymmetric mode peak frequency near 2917 cm^{-1} has been measured in the alkyl polycrystalline state,[18,21] and is often cited as a benchmark indicator of the all-trans conformation.[7,9,12] Peak widths will also increase to reflect an increased distribution of conformational states.[17,18]

More specifically, one must consider that the spectral envelope consists of several modal contributions, the amplitudes of which for some are not directly related to the number of backbone methylene groups. For example, there are Fermi resonance modes and those modes associated with next-to-endgroup vibrations.[18,21] An example of the latter is
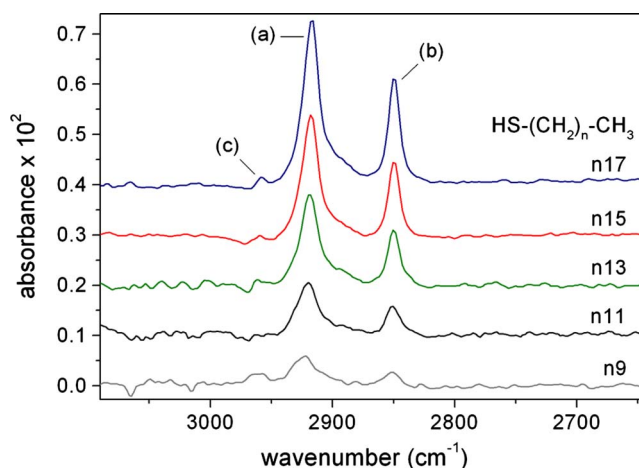

FIG. 1. (Color online) Transmission FTIR spectra of n-alkanethiol [$HS-(CH_2)_n-CH_3$] SAMs on GaAs(001): octadecanethiol (n17), hexadecanethiol (n15), tetradecanethiol (n13), dodecanethiol (n11), and decanethiol (n9). CH_2 stretching modes: asymmetric (a), symmetric (b), and CH_3 stretching modes (c). Spectra are differential, baselined with an etched GaAs reference substrate.

located near 2924 cm^{-1} and corresponds to the asymmetric CH_2 vibration adjacent to sulfur.[28] The distribution of these modes contributes to the apparent position of normal mode peak frequencies that for lower values of n weigh more significantly. Consequently, we will consider the asymmetric mode peak amplitude as a generalized feature of the SAM independent of its precise frequency, with the implicit observation that the spectral envelope contains within it certain constant factors independent of n.

In order to justify this assertion, the correspondence of mode distribution with envelope peak position and amplitude was studied in detail. Using similar peak assignments and a 60/40 Gaussian–Lorentzian line shape mixing ratio as adopted by Parikh and Allara[21] for the polycrystalline alkane $C_{19}H_{39}CO_2Na$, an analytical representation of the CH_2 band was developed and fitted to the spectrum of n17-SAM in the manner described in their report. The component assignments are listed in Table I and the resulting spectrum fit is illustrated in Fig. 2 (top left panel). The model was set to scale with an arbitrary factor (s) parametrized according to the intensity of n-dependent components, leaving the end-group associated elements fixed in amplitude (see mode designations in Table I). Under this first-order assumption, the remaining spectral envelopes were fitted by varying the s-factor, the exception being the n9 spectrum owing to a loss of fidelity. The results from the analysis of the n15, n13, and n11 spectra are shown in the remaining panels of Fig. 2. Agreement is good for the CH_2 asymmetric and symmetric modes, but, for example, the CH_3 mode intensity near 2959 cm^{-1} does not conform well to the applied model, especially as the value of n decreases, because of the initialization of conformational defects that first tend to form at the chain ends.[17,18,29]

The spectrum model may now be used to evaluate the wavenumber position of the generalized asymmetric peak as a function of the scale factor s. This calculation is shown in Fig. 3 along with the data points corresponding to the real asymmetric peak positions at their respective s-values from

TABLE I. Assignment of C–H modal parameters (adapted from Refs. 21 and 28) and scaling indicator for the spectral components of $[HS-(CH_2)_n-CH_3]$ SAMs on GaAs(001).

Mode description[a]	Position (cm^{-1})	FWHM (cm^{-1})	Scaling[b]
CH$_3$, asym str (ip)	2959	6	f
CH$_3$, asym str (op)	2955	6	f
CH$_3$, sym str (FR)	2932	22	s
CH$_2$, asym str (α)	2924	13	f
CH$_2$, asym str	2917	12	s
CH$_2$, sym str (FR)	2902	25	s
CH$_2$, sym str (FR)	2889	16	s
CH$_3$, sym str	2876	10	f
CH$_2$, sym str (α)	2862	12	f
CH$_2$, sym str (β)	2854	9	f
CH$_2$, sym str	2850	10	s

[a]Abbreviations: ip-in plane (CCC), op-out of plane (CCC), FR-Fermi resonance, asym-asymmetric, sym-symmetric, str-stretching, α-CH$_2$ group adjacent to sulfur, and β-CH$_2$ group adjacent to α.
[b]Refers to fixed (f) or n-dependent (s) amplitude in the scaling model.
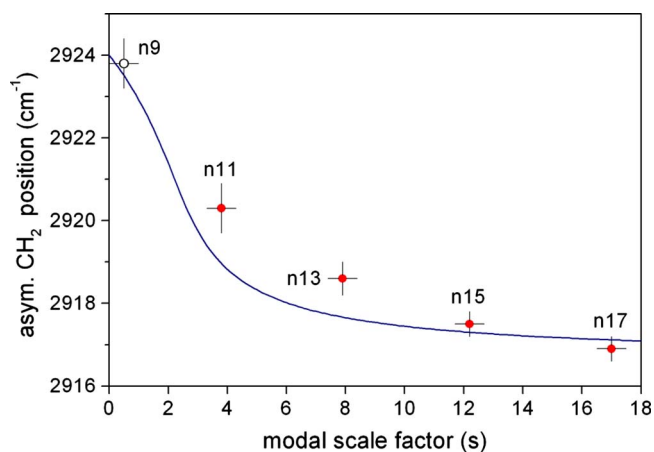

FIG. 3. (Color online) CH$_2$ asymmetric mode peak frequency as a function of the modal analysis scale factor; continuous model (line) and component fit results (circles) illustrating the correspondence of amplitude and peak position in the n-scaling model. Fitting of the n9 spectrum was not possible within the model and its position is estimated only.

the component fit. Note that in the limit of large s, the peak position is asymptotic with 2917 cm^{-1}, i.e., the position associated with the n-dependent CH$_2$ asymmetric stretching mode. For small s, the peak position approaches the value of 2924 cm^{-1} associated with the fixed amplitude component at that position. Deviation of the data points above the analytical curve is observed to increase as the chain length shortens, corresponding to the onset of chain-end *gauche* defects as previously cited. The position of n9 is estimated but is expected to correspond to the frequency limit determined by the dominant 2924 cm^{-1} mode for small s-values. Note the

actual defect fraction responsible for frequency deviations ~ 1 cm^{-1} is less than a few percent.[17,29] Therefore, Fig. 3 indicates that our spectral data and its analytical representation are reasonably self-consistent in terms of amplitude and peak position, validating the component assignments with respect to a near-crystalline phase model for values $n \geq 11$.

Two important conclusions fall out from this discussion. The first is that the validity of n-dependent component scaling supports the physical model upon which the absorption coefficient is based, i.e., that of a uniformly dense SAM changing by molecular length. The second is that generalized
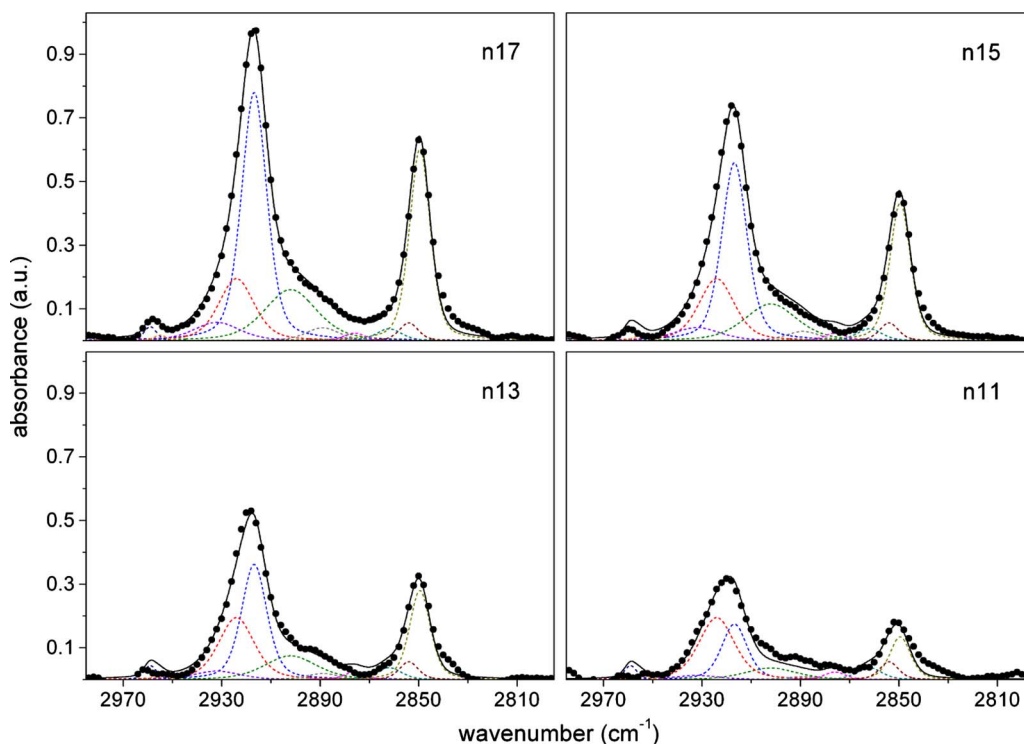

FIG. 2. (Color online) Component analysis of FTIR spectra. Data (circles) and component fit (lines) using fixed and n-dependent C–H stretching mode assignments referenced by peak position in cm^{-1}: 2959 (navy), 2955 (orange), 2932 (violet), 2924 (red), 2917 (blue), 2902 (olive), 2889 (gray), 2876 (magenta), 2862 (dark cyan), 2854 (wine), and 2850 (dark yellow). See Table I for details.
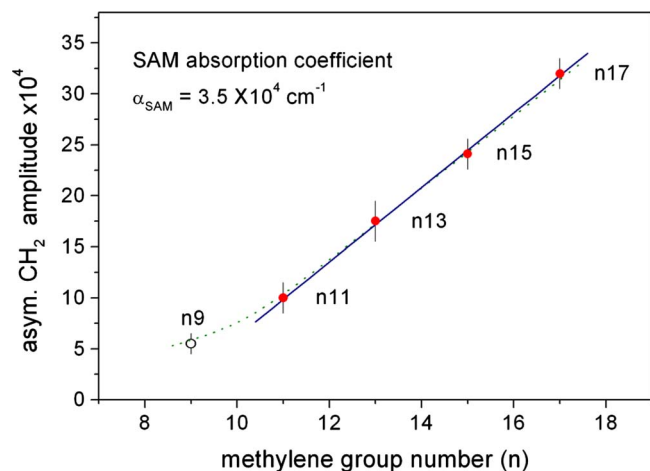
FIG. 4. (Color online) CH$_2$ asymmetric mode amplitude as a function of the methylene group number (circles). Linearization used to derive the absorption coefficient (line). Amplitude scaling model parameterized by the scale factor s to a linear mapping of $n(s)$ (dotted line). Data at $n9$ are predicted for $s<0$ indicating a loss of SAM integrity and marks the assigned threshold n-value.

FIG. 5. (Color online) Example liquid phase CH$_2$ stretching mode spectra: (a) $n13/11$ μm, (b) $n9/8$ μm, and (c) $n13/4$ μm, according to measured layer thickness. Absorption coefficients are derived from the asymmetric mode peak amplitudes, e.g., α_{n9} and α_{n13}. The ratio of points (i) and (ii) verify the linear dependence of absorbance on layer thickness, in this case for $n13$.

comments about the quality of the SAM, in terms of the fraction of conformational defects, should not hinge upon the asymmetric peak position in its entirety, at least not for comparison between SAMs of two different molecular lengths.

As an aside, it should be mentioned that our SAMs were incubated on both the front and back sides of polished wafers. Therefore, the absorbance magnitudes scale by a factor of 2 when measured in transmission, increasing the signal-to-noise ratio. This was confirmed by an experiment where only one side of a wafer was etched before incubating in $n17$. The resulting peak amplitude was reduced by a factor of 2 as expected, since the SAM will not form on the oxidized surface.

IV. STRUCTURAL THRESHOLD AND ABSORPTION COEFFICIENTS

The asymmetric peak amplitude as a function of the methylene group number n is plotted in Fig. 4. The linearity of the data is immediately apparent and is consistent with the physical model prefaced in Sec. III. Also shown in Fig. 4 is the amplitude n-scaling model parametrized by the scale factor s to a linear mapping of $n(s)$ between $n11$ and $n17$. Agreement is excellent, and moreover, extrapolation of the model to $s<0$ (between $n=9$ and $n=10$) simulates the loss of SAM integrity and predicts a trend consistent with the position of the $n9$ data. Consequently, we are justified in adopting the values $n>9$ in defining a structural regime of well ordered self-assembly.

Using ellipsometric and angle-resolved x-ray photoelectron spectroscopy (XPS) data, an earlier report[4] suggested a SAM threshold in the vicinity of $n=13$. Sample preparation techniques, which the present study employs, have recently been improved by McGuiness et al.[7] Characteristic of this improvement is a significant decrease in molecular tilt from 57° to 14° for $n17$.[7] Corroborating results have been reported for SAMs with chain lengths ranging from $n11$ to $n17$.[13] The linearity of the data in Fig. 4 confirms that the expected
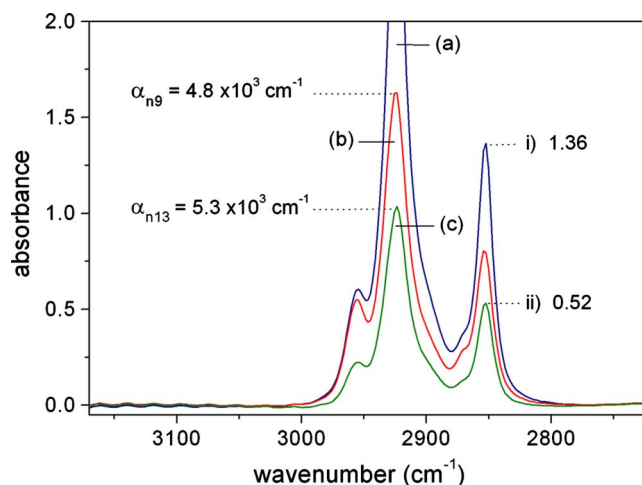
increase in molecular packing and chain overlap afforded by a lower value of molecular tilt enables better structural coherence at shorter chain lengths than was previously reported.

Having justified the validity of the physical model, the linearity of absorbance with SAM molecular length enables the absorption coefficient to be derived. Taking a slope of 3.7×10^{-4} absorbance units per unit n from Fig. 4, normalizing by 1.54 sin 55° Å, which is the C–C bond length (per CH$_2$ unit) projection along the molecular axis, multiplying by $1/\cos(14°)$ to account for the assumed molecular axis tilt, and considering the aforementioned 2× multiplier, the coefficient value thus obtained is $\alpha_{SAM}=3.5 \times 10^4$ cm^{-1}. It should be noted that our value of α_{SAM} corresponds to the maximum point in the CH$_2$ stretching mode region. A frequency spectrum of the absorption coefficient $\alpha(\nu)$ could easily be constructed by normalization of the CH$_2$ spectral maximum to the α_{SAM} value.

Note that recent work by McGuiness et al.[9] has reported some loss of SAM coverage and organization for values of $n<15$ in this material system. Our present results are consistent with their comments in terms of structural organization, having observed a similar increase in gauche defects at lower n-values as discussed above. Additionally, the loss of coverage with decreasing n-value they reported (up to 12% for $n11$) may be superimposed on our data, but in a slowly varying manner beyond the sensitivity of our method. Owing to the slope error such a case would impart, it is possible that the α_{SAM} value may be overestimated by up to 5%.

In order to compare α_{SAM} to the bulk state, liquid phase Beer–Lambert measurements were carried out to explicitly determine the respective absorption coefficients for several n-values.[27] Measured liquid layer thicknesses ranged from 4 to 11 μm and it was observed that the ratio of amplitudes between spectra of a given n-value corresponded by ratio of thickness as expected for linear attenuation, as the example of Fig. 5 illustrates for $n13$. Next, each absorption coefficient
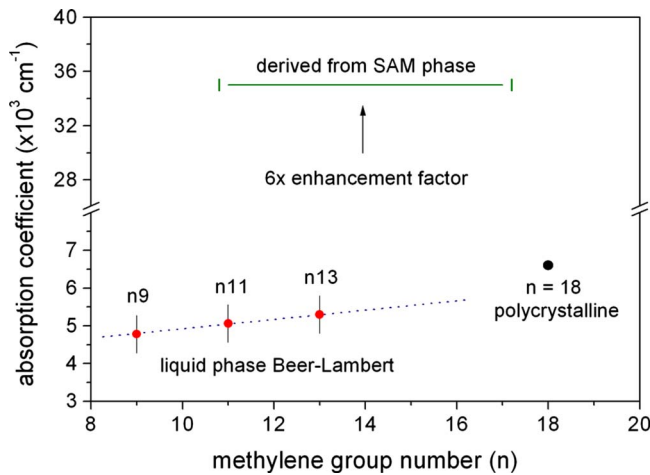
FIG. 6. (Color online) Enhancement factor observed for the SAM phase absorption coefficient relative to Beer–Lambert measurements in bulk material. Data at $n=18$ evaluated from the spectrum of k for polycrystalline $C_{19}H_{39}CO_2Na$ in Ref. 21. The dotted line is used for trend visualization only.

was calculated referencing the asymmetric peak amplitude and measured layer thickness data, the results of which are reported in Fig. 6, along with the constant value of α_{SAM} derived above. Also shown in Fig. 6 is a data point borrowed from Parikh and Allara,[21] evaluated from the spectrum of k (imaginary part of the refractive index) in a KBr dispersed IR measurement of polycrystalline $C_{19}H_{39}CO_2Na$. Figure 6 provides a graphical representation of the $6\times$ enhancement factor observed between the liquid and SAM phase absorption coefficients.

V. ABSORPTION ENHANCEMENT EFFECT

The liquid phase trend line in Fig. 6 suggests that polycrystalline phase absorption coefficients may be up to 10% higher approximately. However, reported transmission FTIR measurements of the solid-liquid phase transition in polycrystalline n-$C_{21}H_{44}$ thin films (2–10 μm) has demonstrated an intensity reduction of about 30% upon melting.[30] Some decrease is expected owing to the lower number density, loss of intermolecular interaction, and increased conformational disorder associated with the liquid state.[30,31] We shall assume that our liquid phase absorption coefficients reflect these intrinsic factors to a degree corresponding to the larger estimate, i.e., we expect up to a 40% increase in absorbance upon the crystalline phase transition.

Now consider the effect of number density. Based on the specific gravities and molecular masses of $n11$ and $n13$, their respective number densities are 2.5×10^{21} cm^{-3} and 2.2×10^{21} cm^{-3}. Given these values, in a volume corresponding to their molecular length, about 15 and 18 Å, respectively, the areal densities each evaluate to approximately 0.04 Å^{-2}. Also consider that the ideal SAM maintains a close-packed separation of about 4.5 Å, i.e., the molecular diameter, in a manner consistent with the polycrystalline state. In terms of an assumed square lattice surface cell, this yields an areal density of 0.05 Å^{-2} and we may conclude that the SAM

density is greater than the liquid by about 25%, accounting for a significant fraction of the 40% increase expected based on the phase change from the liquid state.

A more significant factor to address is the spatial orientation of the molecules with respect to the polar orientation of the incident optical wave. It is well known that the intensity of the vibrational transition is proportional to $|\mathbf{E} \cdot \mathbf{p}|^2$, where $\mathbf{E}$ is the electric-field vector of the IR optical probe and $\mathbf{p}$ is the transition dipole moment (discussed in Refs. 21 and 22). For the case of an isotropic liquid, averaging the $\cos^2$ term over 4π yields a factor of 1/3, relative to the case of a fixed molecular orientation of $\mathbf{p}$ collinear with $\mathbf{E}$ (the maxima). In the SAM, the normal coordinates for both the asymmetric and symmetric vibrations are near coplanar with the surface, given that they are both directed orthonormal to the molecular axis and that the molecular axis tilt is small (15°) with respect to the surface normal. Since our spectra were taken with unpolarized light, we may average in the plane of $\mathbf{E}$ for measurements made in transmission, resulting in a factor of 1/2 for the SAM phase. Therefore, based on orientational considerations, the maximum absorbance scale factor expected for the SAM relative to the liquid phase in our measurements is about 1.5$\times$.

The combined effects of phase transition and orientation have accounted for about 2$\times$ of the 6$\times$ enhancement factor observed in the data. The remainder can be accounted for by considering the possible extrinsic effects of the surface or of intermolecular interactions specific to the SAM phase. Since the value of $\mathbf{p}$ is described classically as being proportional to the dipole moment derivative with respect to the normal coordinate of vibrational oscillation,[21,32] factors significant to a redistribution of electron density, such as molecular orbital intermixing and van der Waals forces, may result in increased oscillator strength, namely, $|\mathbf{p}_{SAM}| > |\mathbf{p}_{liq}|$. The contribution of such factors stands to the reason given the important role of intermolecular forces driving the self-assembly mechanism,[17,33,34] and follows naturally from the discussion of phase related intensity variation outlined above. Note that in general, $\Delta\mathbf{p}$ may occur by virtue of a change in net permanent dipole or by induced dipole effects, i.e., a change in vibrational polarizability.[35]

In view of these considerations, two surface mechanisms can be included in the list of extrinsic factors expected to affect a redistribution of electron density. First is the sheet dipole moment contribution to the surface potential and second is the charge transfer associated with chemisorption of the thiol group to the GaAs(001) surface. A chain-length dependent dipole potential of about 230 mV is expected for $n17$-SAMs on GaAs(001),[12] based on measurements of $n17$-SAMs on Au.[36] In addition, XPS analysis has demonstrated an estimated 1.5 eV reduction in the binding energy of the S $2p$ line upon thiol chemisorption in $n17$-GaAs(001) SAMs,[4,7] indicating significant charge transfer from the surface upon covalent bond formation. Other surface potential factors may play a role, such as those stemming from uncompensated semiconductor surface states. These factors will contribute to a chemical state modification of the surface

environment, possibly resulting in a change of polarization sufficient to account for the observed absorption enhancement.

While this discussion does not refer to specific mechanisms other than factors relevant to a scaling of the generalized selection rule for IR activity, our results can be placed in the context of similar observations made in other material systems. For example, chemisorption has been demonstrated as a distinguishing feature of IR enhancement on planar metal surfaces, such as the four times increase in vibrational polarizability observed for CO chemisorbed on Cu and Ag, compared to its gas and physisorbed phases.[37,38] Moreover, enhancements of the order $10-10^3$ can be realized on rough metal or metal-particle substrates in surface enhanced infrared absorption (SEIRA) techniques,[32] and has been observed for $n17$ adsorbed on Au islands specifically.[39] Both electromagnetic (plasma resonance) and chemical mechanisms account for the observed SEIRA enhancements and research distinguishing the two has been reported,[32,40] concluding that (1) scaling of order 10 can be achieved based on the chemical mechanism and that (2) chemisorption is a required element for this to manifest. An explanation behind the chemical mechanism has been described for the case of CO chemisorbed on Cu(001) and relates to a dynamic charge transfer between adsorbate and metal bonding orbitals.[41] The chemical mechanism in SEIRA is less well understood but is thought to relate in a similar manner.[32]

Considering the expected change in chemical environment upon SAM formation and particularly its dependence on thiol chemisorption, the similarity in the extrinsic enhancement factor $(3\times)$ relative to metal-based observations suggests that a related chemical mechanism may exist on the semiconductor surface. It is hoped that our results will add to the data supporting such effects and to corresponding refinements in theoretical hypotheses.

VI. CONCLUSIONS

SAM phase FTIR measurements of various n-alkanethiols on SI-GaAs(001) were made. Component analysis of the CH_2 stretching mode region demonstrated good correspondence between the peak position and amplitude, supporting a structurally coherent physical overlayer model in the absence of significant conformational defects. Linearization of the asymmetric peak amplitude with molecular chain length yielded an absorption coefficient maximum of 3.5×10^4 cm^{-1} and provided evidence of ordered self-assembly for n-values >9. Enhancement of the absorption coefficient was quantified to be $6\times$ relative to the polycrystalline and liquid phases. About $2\times$ of this enhancement factor was accounted for by the crystalline phase transition and molecular orientation, with the remainder attributed to the influence of surface and intermolecular effects specific to the SAM phase. As a more direct measurement of the absorption coefficient, our results are relevant to the accuracy of surface derived quantities and demonstrate the significance of the chemical environment on IR spectral intensity.

[1]O. S. Nakagawa, S. Ashok, C. W. Sheen, J. Märtensson, and D. L. Allara, Jpn. J. Appl. Phys., Part 1 **30**, 3759 (1991).

[2]C. W. Sheen, J. X. Shi, J. Märtensson, A. N. Parikh, and D. L. Allara, J. Am. Chem. Soc. **114**, 1514 (1992).

[3]K. Adlkofer and M. Tanaka, Langmuir **17**, 4267 (2001).

[4]Y. Jun, X. Y. Zhu, and J. W. P. Hsu, Langmuir **22**, 3627 (2006).

[5]S. Ye, G. Li, H. Noda, K. Uosaki, and M. Osawa, Surf. Sci. **529**, 163 (2003).

[6]Q. Zhang, H. Huang, H. He, H. Chen, H. Shao, and Z. Liu, Surf. Sci. **440**, 142 (1999).

[7]C. L. McGuiness, A. Shaporenko, C. K. Mars, S. Uppili, M. Zharnikov, and D. L. Allara, J. Am. Chem. Soc. **128**, 5231 (2006).

[8]C. L. McGuiness, A. Shaporenko, M. Zharnikov, A. V. Walker, and D. L. Allara, J. Phys. Chem. C **111**, 4226 (2007).

[9]C. L. McGuiness, D. Blasini, J. P. Masejewski, S. Uppili, O. M. Cabarcos, D. Smilgies, and D. L. Allara, ACS Nano **1**, 30 (2007).

[10]O. Voznyy and J. J. Dubowski, J. Phys. Chem. C **112**, 3726 (2008).

[11]D. M. Wieliczka, X. Ding, and J. J. Dubowski, J. Vac. Sci. Technol. A **24**, 1756 (2006).

[12]S. Lodha and D. B. Janes, J. Appl. Phys. **100**, 024503 (2006).

[13]G. Nesher, A. Vilan, H. Cohen, D. Cahen, F. Amy, C. Chan, J. Hwang, and A. Kahn, J. Phys. Chem. B **110**, 14363 (2006).

[14]L. Mohaddes-Ardabili, L. J. Martínez-Miranda, J. Silverman, A. Christou, L. G. Salamanca-Riba, and M. Al-Sheikhly, Appl. Phys. Lett. **83**, 192 (2003).

[15]X. Ding, K. H. Moumanis, J. J. Dubowski, E. H. Frost, and E. Escher, Appl. Phys. A: Mater. Sci. Process. **83**, 357 (2006).

[16]X. Ding, K. Moumanis, J. J. Dubowski, L. Tay, and N. L. Rowell, J. Appl. Phys. **99**, 054701 (2006).

[17]L. H. Dubois and R. G. Nuzzo, Annu. Rev. Phys. Chem. **43**, 437 (1992).

[18]R. G. Nuzzo, L. H. Dubois, and D. L. Allara, J. Am. Chem. Soc. **112**, 558 (1990).

[19]D. Li, B. I. Swanson, J. M. Robinson, and M. A. Hoffbauer, J. Am. Chem. Soc. **115**, 6975 (1993).

[20]I. Zawisza, A. Lachenwitzer, V. Zamlynny, S. L. Horswell, J. D. Goddard, and J. Lipkowski, Biophys. J. **85**, 4055 (2003).

[21]A. N. Parikh and D. L. Allara, J. Chem. Phys. **96**, 927 (1992).

[22]D. L. Allara and R. G. Nuzzo, Langmuir **1**, 52 (1985).

[23]S. Flink, F. C. J. M. van Veggel, and D. N. Reinhoudt, Adv. Mater. (Weinheim, Ger.) **12**, 1315 (2000).

[24]M. V. Lebedev, D. Ensling, R. Hunger, T. Mayer, and W. Jaegermann, Appl. Surf. Sci. **229**, 226 (2004).

[25]C. Bryce and D. Berk, Ind. Eng. Chem. Res. **35**, 4464 (1996).

[26]Sample preparation carried out in a nitrogen purged glovebox mitigated the negative effects of humidity and oxidation as described in Ref. 7. This was particularly relevant in order to achieve good results for SAMs $n < 15$.

[27]Alkanethiols $n15$ (solid/liquid) and $n17$ (solid) cannot be measured in the liquid phase at room temperature.

[28]K. D. Truong and P. A. Roundtree, J. Phys. Chem. **100**, 19917 (1996).

[29]J. Hautman and M. L. Klein, J. Chem. Phys. **93**, 7483 (1990).

[30]H. L. Casal, D. G. Cameron, and H. H. Mantsch, Can. J. Chem. **61**, 1736 (1983).

[31]D. L. Allara, personal communication (14 May 2008).

[32]M. Osawa, in *Near-Field Optics and Surface Plasmon Polaritons*, Topics in Applied Physics Vol. 81, edited by S. Kawata (Springer-Verlag, Berlin, 2001), p. 163.

[33]J. Hautman and M. L. Klein, J. Chem. Phys. **91**, 4994 (1989).

[34]A. Ulman, J. E. Eilers, and N. Tillman, Langmuir **5**, 1147 (1989).

[35]H. Torii, J. Comput. Chem. **23**, 997 (2002).

[36]S. Howell, D. Kuila, B. Kasibhatla, C. P. Kubiak, D. Janes, and R. Reifenberger, Langmuir **18**, 5120 (2002).

[37]B. N. J. Persson and A. Liebsch, Surf. Sci. **110**, 356 (1981).

[38]P. Dumas, R. G. Tobin, and P. L. Richards, Surf. Sci. **171**, 555 (1986).

[39]D. Enders and A. Pucci, Appl. Phys. Lett. **88**, 184104 (2006).

[40]M. Osawa and M. Ikeda, J. Phys. Chem. **95**, 9914 (1991).

[41]B. N. J. Persson and R. Ryberg, Phys. Rev. B **24**, 6954 (1981).